Journal of Chemical Science and Engineering
JCSE, 2(2): 61-69
www.scitcentral.com

ISSN: 2642-0406

Review Article: Open Access

Birnessite-Related Manganese Nano-Oxides: Dopant Location, a Key Factor to understand their Properties

A Azor[1], I Gómez-Recio[1], L Ruiz-González[1], M Parras[1], JM González-Calbet[1,2*]

[*1]*Department of Inorganic Chemistry, Complutense University of Madrid, Madrid, Spain*

[2]*National Center for Electron Microscopy, Complutense University of Madrid, Madrid, Spain.*

Received February 08, 2019; Accepted March 22, 2019; Published May 20, 2019

ABSTRACT

Birnessite related layered manganese oxides are a versatile family of compounds. Here we summarize the wide range of applications that these phases have and the numerous synthesis strategies proposed for their production at the nanoscale. Doping these manganese oxides with other transition elements have revealed as one of the most successful strategies to improve their properties but a direct tool to determine where these dopants are located is still needed. We present here our approach to the synthesis of doped ultrathin birnessite nanoparticles and an atomic resolution electron microscopy study in order to elucidate the positions that the foreign cations occupy.

Keywords: Birnessite, Layered nanomaterials, HRTEM, Soft-chemistry, EELS

INTRODUCTION

Transition metal oxides form the basis of a large number of functional devices that are part, among others, of environmental, energy and information technologies. Many of these oxides crystallize in structural types that can be modified by the introduction of small compositional and/or structural variations. This aspect deserves particular attention since ionic defects can play a key role in the development or improvement of a certain functional behavior of these materials. On the idea, well established, that slight variations in the composition can be the origin of remarkable changes in a certain property, it should be noted that the ease that have some structural types to promote the mobility of oxygen ions and cause anionic deficiency, can lead to develop new strategies that could modify or improve the functional behavior of many of these materials. Among the transition metals, the best candidates to satisfy this behavior are those first transition metals able to adopt several oxidation states and several coordination environments. One of the most versatile is Mn, which due to the ability of developing these capabilities, combined with its electronic behavior gives rise to a wide range of applications as catalysts [1], ionic and electronic conductors [2], magneto-resistant materials [3], etc. Most of these studies have been devoted to three-dimensional manganese oxides, in particular those related to the perovskite structural type. Nevertheless, in the last years there has been an increasing activity in the search of more open structures easing the interchange and ion mobility. In this scenario, manganese can also be stabilised in layered structures. This is the case of birnessite related compounds that can play a paramount role in catalytic and environmental applications.

The birnessite-structured manganese dioxide, δ-MnO_2, is a polymorph of the MnO_2 family. Its layered structure can be described as sheets of edge-sharing MnO_6 octahedra, interleaved by diverse cations and water molecules **(Figure 1)** [4]. The mineral that this family is named after ($(Na_{0.7}Ca_{0.3})Mn_7O_{172.8}H_2O$) usually has low crystallinity [5], so, the structural characterization of this phase could not be possible until Post et al. [6] produced a synthetic sodium birnessite. The δ-MnO_2 crystallizes in a C2/m spatial group with the following parameters: a=5.174 Å, b=2.850 Å, c=7.336 Å and β=103.18° [6]. The oxidation state of manganese is III and IV, leading to charged layers. This negative charge is compensated by interlaminar cations, usually alkali or alkaline earth metals [6], but transition metal and rare earth interleaved birnessites have also been

Corresponding author: José María González Calbet, Department of Inorganic Chemistry, Faculty of Chemistry, Complutense University of Madrid, Madrid-28040, Spain, E-mail: jgcalbet@ucm.es

Citation: Azor A, Gómez-Recio I, Ruiz-González L, Parras M & González-Calbet JM. (2019) Birnessite-Related Manganese Nano-Oxides: Dopant Location, a Key Factor to understand their Properties. J Chem Sci Eng, 2(2): 61-69.

reported [7-9]. On the other side, the defects most commonly found are anionic vacancies as well as migration of manganese cations into the interlayer space [10].

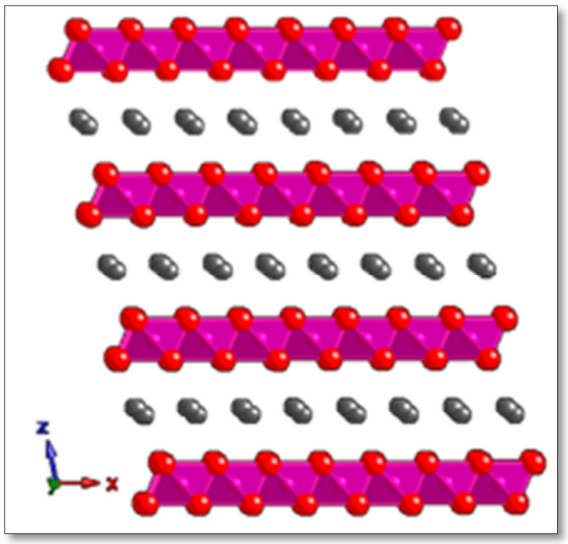

Figure 1. Model of the birnessite structure.
K: Grey, Mn: Magenta and O: Red

PROPERTIES AND APPLICATIONS

The natural birnessite is an abundant phase in any kind of soils, especially in oceanic ones, recovering deposits of other minerals as high specific surface aggregates [7]. The chemical influence of birnessite, like other manganese oxides, plays a key role on regulation of heavy metals concentration in the waters of our planet. These phases act as natural traps of metallic cations dissolved in rivers and oceanic waters [11], thanks to their ability of absorbing them on their structure. Therefore, the mineral birnessite is used in wastewater remediation pools in mineral exploitations [12]. The high reactivity of these oxides also benefits their environmental activity, mainly as oxidizing agent of different pollutants. For example, birnessite is able to oxidize the toxic As(III) to As(V), an specie much easier to eliminate by conventional water treatment methods [13].

The most common applications of the synthetic birnessite, like the natural one, make use of their ionic exchange properties [14]. The birnessite phases, intercalated with different monovalent cations, are able to reach topotactic exchange ratios of 80-90%. This means that the birnessite structure suffers only changes in its basal distance between MnO_2 layers, capturing and releasing a great number of different kinds of dissolved cations. Therefore, nowadays, the main technological application of synthetic birnessite is, again, heavy metals removal from polluted waters.

The high ion mobility in birnessite structure allows these phases to be used as electrodes for lithium or sodium batteries [15,16]. In the former, depending on the synthesis method, capacities in the order of 200 mA $h \bullet g^{-1}$ can be obtained [17]. Nevertheless, these electrodes seem to suffer some degradation problems but, after several charge/discharge cycles, the material keep capacities around 150 mA $h \bullet g^{-1}$ for long periods. The main efforts to improve the electrochemical performance of these oxides are focused on the partial substitution of Mn by other transition metals. For example, the inclusion of a small amount of Ni in a lithium birnessite increases the electrode capacity to 213 mA $h \bullet g^{-1}$ even after 80 cycles [18]. Recently, Na ion batteries have been intensively studied as an interesting alternative for certain applications. In this field, birnessite based electrodes are again promising candidates. The material response can be modulated by controlling the intercalated water in the structure. Recent works, as the one published by Zhu et al. [16], proof that highly hydrated sodium birnessites show a charge capacity 190% greater than the dehydrated phase, keeping it after several cycles.

Electrochemical capacitors, also known as supercapacitors, have shorter charge/discharge times releasing much greater currents in shorter times and larger operational life [19,20]. A sodium ion battery coupled with supercapacitors could configure a flexible energy-storing device with multiple applications. A supercapacitor is based on a double layer configuration that stores energy in the solid electrolyte interlayer without chemical reactions. Potassium birnessite shows a promising behavior since the bulk oxide, with very low surface area, reach capacitance values of 110 $F \bullet g^{-1}$ [21]. The performance of this material can be improved substituting some Mn for vanadium [22]. Doping the oxide with 15% of V increases the capacitance to 246 $F \bullet g^{-1}$ after 200 cycles.

One of the most encouraging research fields on new energy conversion systems are reversible solid-state fuel cells (RSOFCs). RSOFCs are single-unit, all solid-state, electrochemical devices that can operate in both the fuel cell (SOFC) and electrolysis (SOEC) mode. It is an energy conversion and storage system especially appropriate to store intermittent renewable energy, such as wind or solar [23]. A suitable candidate to integrate one of these devices have to be active either in the oxygen evolution reaction (OER), when the cell is operated in SOEC mode and oxygen reduction reaction (ORR) for the SOFC mode. Birnessite oxides have been tested in both reactions separately [24,25]. Therefore, these compounds could constitute appropriate electrodes for RSOFCs but, as far as we know, this possibility has not been explored. On one hand, theoretical studies evidence that the interactions between the interlayer cations and the water molecules diminish the OER activation energy. Therefore, the electrocatalytic performance of the birnessite system can be improved intercalating electrocatalytically active transition metals like Ni [8], Co [26] or Cu [27]. On the other hand, like other MnO_2 polymorphs, birnessite oxides are active in ORR and have a significant electric conductivity [25,28].

As it will be discussed later, several different synthesis methods have been developed to produce birnessite nanoparticles and, therefore, with high specific surface area. This, combined with the known catalytic activity of other manganese oxides, has encouraged the scientific community to test the catalytic behavior of different birnessite phases on various reactions. The birnessite oxides are active in formaldehyde oxidation. The molecule can be produced, under certain humidity and temperature conditions, by degradation of wood furniture varnishes. This can be avoided adding a small portion of birnessite oxide to the preparation [9,29,30]. Birnessite phases are also active on CO oxidation, improving their behavior when a portion of the manganese is substituted by other transition metals [31]. Nevertheless, their low thermal stability limits their activity.

SYNTHESIS METHODS AND REACTIVITY

There are numerous synthesis methods to produce birnessite. The first procedure was based in a solid-state reaction to obtain a bulk material [6] and, thereafter, there have been some efforts to synthesize large monocrystals using flux methods [32]. Nevertheless, with the applications discussed above in mind, the birnessite behavior could be improved with a nanostructured material. There are two soft chemistry routes to obtain birnessite nanosheets. The first synthesis pathway is a room-temperature co-precipitation method using manganese (II) sulfate or nitrate in a basic media (usually a NaOH or KOH solution in order to produce the sodium or potassium phase, respectively), in presence of an oxidizing agent like hydrogen peroxide or sodium thiosulfate [33]. The second procedure involves the reaction between potassium permanganate and hydrochloric acid at 80-100°C and its subsequent ageing at 50-60°C for 15 h [10]. The former yields aggregated small nanoparticles, whereas the later leads to nanoflowers made by birnessite nanosheets. Both methods allow the partial substitution of the manganese by other elements. We have found in the literature Co [26], Cr [34] and V [22] doped birnessite nanoparticles by these procedures, and our group, as will be discussed later, have adapted the basic co-precipitation method to produce Fe, Ti and Ce doped phases. While the co-precipitation method produces the smallest nanoparticles and seems to be more flexible in terms of manganese substitution, the KMnO4 reaction can be modified to synthesize complex architectures. For example, Portehault et al. [10] designed core-corona nanoparticles introducing Mn (II) in the acidic mixture and adjusting the aging time and temperature. In this case, the particles are made by an amorphous MnO_2 core surrounded by birnessite nanosheets. Zhu et al. [35] produce ultrathin parallel birnessite nanosheets grown onto MnO_2 nanowires; aging the acidic $KMnO_4$ solution with MnOH nanowires as sheds.

Apart from these two common methods, some other synthesis pathways have been developed. Ching et al. [36] published a sol-gel method using $KMnO_4$ and glucose to form the gel that is subsequently calcined. Nevertheless, this procedure yields larger particles than the previous ones. There are also hydrothermal routes studied for this system, like the one proposed by Zhang et al. [37]. This method drives to porous birnessite nanoflowers with high specific surface area for their application as supercapacitors. Komaba et al. [38] found that, while testing the electrochemical performance of some Mn (III) based oxides, the activity of the material was significantly improved after the first cycle. The structural analysis revealed that the initial material had been modified producing birnessite nanoparticles, being this new phase responsible of the improved behavior.

Like other 2D materials, birnessite can undergo ion exchange reactions and, under certain conditions, the structure can be delaminated into disperse monolayers. The ion exchange reactions take place simply by soaking the oxide with a concentrated solution of the cation that wants to be intercalated. In this way, Co [24], Ni [8] or Cu [27] interleaved birnessites can be prepared. When the intercalated cation is large enough, mostly bulky amines like tetrabutylammonium (TBA), the interaction between layers is weak enough that the monolayers can be suspended in the appropriate solvent [39,40].

Other interesting feature of the birnessite related oxides is that can be transformed into different channel MnO_2 structures by a hydrothermal method [33]. The final channel structure depends on which cation occupies the interlayer space, the temperature and the acid used in the hydrothermal method. Although the exact mechanism is still unknown, the layer structure seems to collapse around the interlayer cation forming the channel along the final structure. The size of this channel is templated by the interlayer cation. So, starting from a compositionally controlled birnessite, a well-defined tunnel structured manganese oxide can be achieved. These tunnel structures, like pyrolusite or hollandite, are well known as promising functional materials [41,42] and their particle size, morphology and composition could be controlled by using the right birnessite precursor.

SEARCHING FOR THE DOPANT LOCATION

Our current work is focused on either synthesize nanostructured birnessites doped with Fe, Ti and Ce and shed light over where the dopants are located by using atomic resolution electron microscopy. The obtained birnessites are meant to be used as solid precursors for hollandite structured nanowires. As previously mentioned, these tunnel structures have attractive properties, their catalytic activity being one of the most relevant [42]. Besides, as previously mentioned, Co, Cr and Cu doped birnessite phases have also been reported. On the basis of this information, we thought that Fe or Ti, known catalytically active elements [43,44], could be adequate dopants to improve the performance of the final material. Ce is also a quite catalytically active element, and its inclusion in the manganese oxide framework can enhance its behavior.

At the same time, we find that, as far as we know, there is some lack of precision defining where the dopants are located in the oxide structure. Most authors rely on indirect methods to induce where the dopants are but, even when they are probably right; their conclusions are subject to interpretation. We have tried to find the appropriate conditions for a direct visualization of the structure of the birnessite nanoparticles by atomically resolved transmission electron microscopy (HRTEM) and, at the same time, analyze their local composition by scanning transmission electron microscopy (STEM) and electron energy loss spectroscopy (EELS).

We have chosen the co-precipitation method to produce our birnessite nanoparticles. The procedure consists in the injection of a 1 M $Mn(NO_3)_2$•$4H_2O$ (99.99%, Sigma-Aldrich) solution into a mixture of 50 ml KOH (99.99%, Sigma-Aldrich) solution 0.8 M with 1.02 ml of H_2O_2 (30%, Sigma-Aldrich) at room temperature under vigorous stirring. A brownish black precipitate forms immediately, which is washed with water and recovered by centrifugation. In order to produce Fe, Ti or Ce doped phases, the manganese nitrate solution should be substituted by the corresponding mixture of this precursor plus $Fe(NO_3)_3$•$9H_2O$ (99.99%, Sigma-Aldrich), dihydroxybis(ammoniumlactate)titanium (IV) (sol. 50% in water, Sigma-Aldrich) or $Ce(NO_3)_3$ (99.99%, Sigma-Aldrich), respectively.

The average composition of the undoped phase, determined by electron microscopy probe and thermogravimetric analysis, is $K_{0.36}MnO_2$•$0.87H_2O$. X-ray diffraction (XRD) data show low intensity wide diffraction maxima **(Figure 2)** which can be indexed as a birnessite phase (COD 9001272). In the case of the doped phases, the compositional analysis is in agreement with the nominal one. When Fe, Ti or Ce is included in the reaction mixture, the X-ray diffraction pattern shows even wider maxima (not included). The wide nature of the diffraction maxima suggests the presence of nanostructured phases.

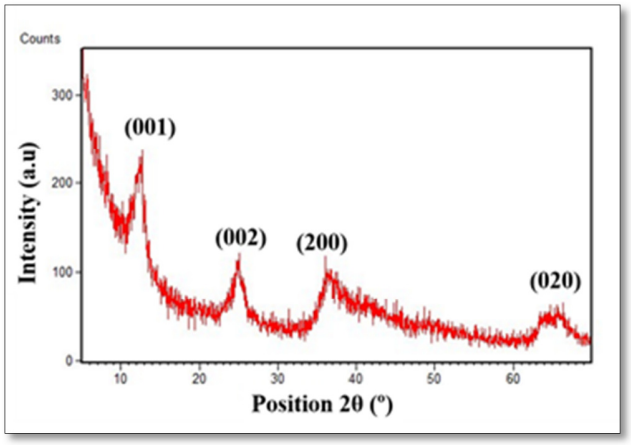

Figure 2. XRD pattern of an undoped sample.

TEM study, performed in two JEOL electron microscopes, JEM 2100 and GRAND ARM, confirms the stabilization of doped and undoped birnessite nanoparticles. Typical low magnification TEM images indicate the presence of very thin and heterogeneous shaped aggregates **(Figure 3a)** which, according to HTREM images, comprise two microstructural features (marked in **Figure 3b** as A and B together with enhanced inset and their corresponding FFT):

A) A polycrystalline matrix, built up from very small particles (5 nm or less), exhibiting a hexagonal distribution of contrasts with 0.53 nm × 0.28 nm periodicities, in agreement with the birnessite unit cell along (001) **(Figure 3c)**.

B) Layered nanostructures, built up from 2-5 layers with typical interlayer distances around 0.7 nm, characteristic of the birnessite lattice along the (100) direction **(Figure 3d)**. The microstructural features here shown correspond to an iron doped sample (5% Fe) but they are present in both doped and undoped samples. Nevertheless, it should be mentioned that, as the dopant is introduced, the ratio of particles orientated perpendicular to the (001) direction increases, which is in agreement with the broadening of the diffraction peaks observed in XRD **(Figure 4)**. This could be explained due to a reduction of the particle size and aspect ratio as a consequence of the inclusion of the dopants, as previously observed in other layered oxides [45].

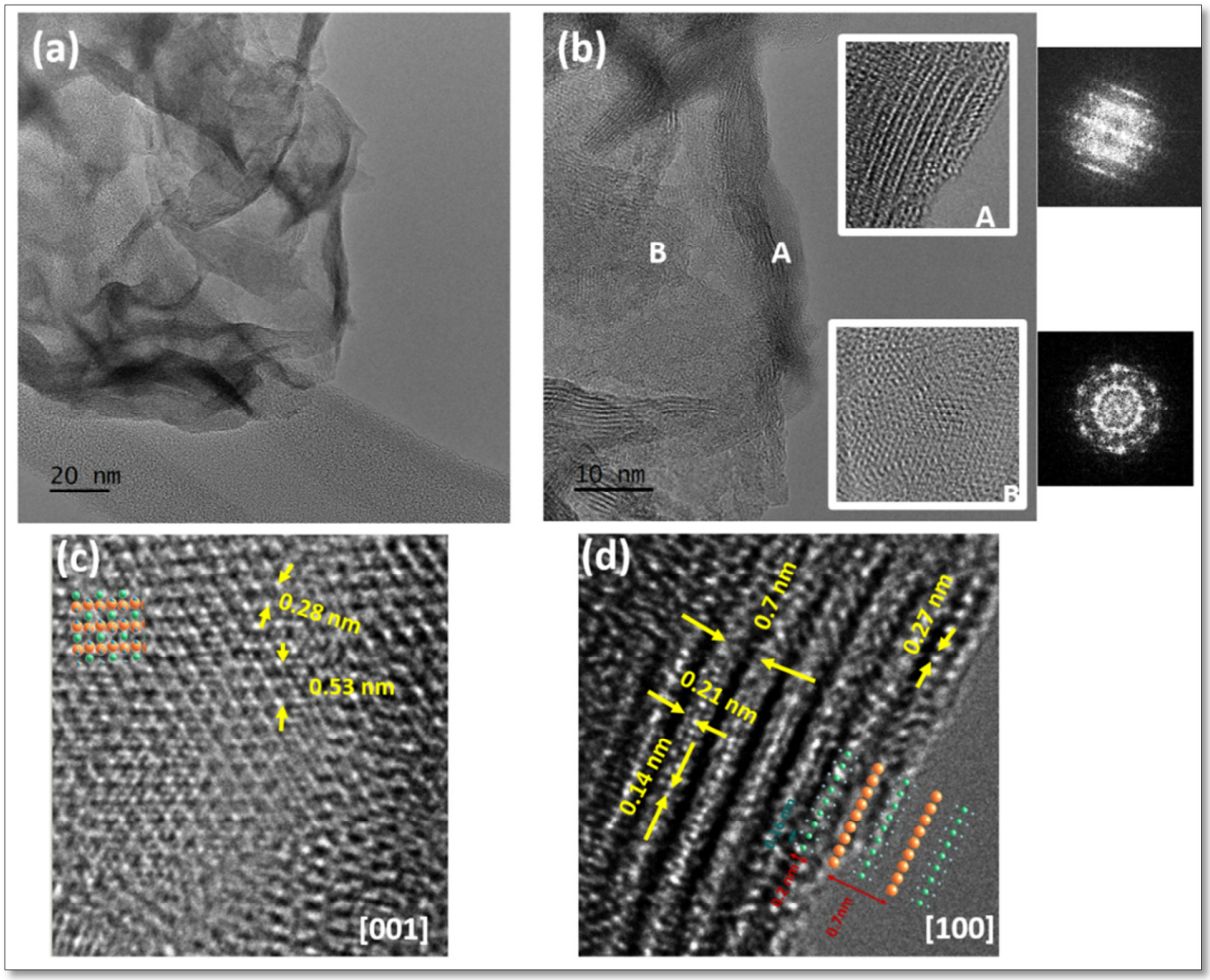

Figure 3. (a) Representative low magnification TEM image of birnessites. (b) HRTEM image showing the two microstructures (marked as A and B and better observed in the insets) present in birmesites. (c) Enhanced details of the A and B features shown in (b).

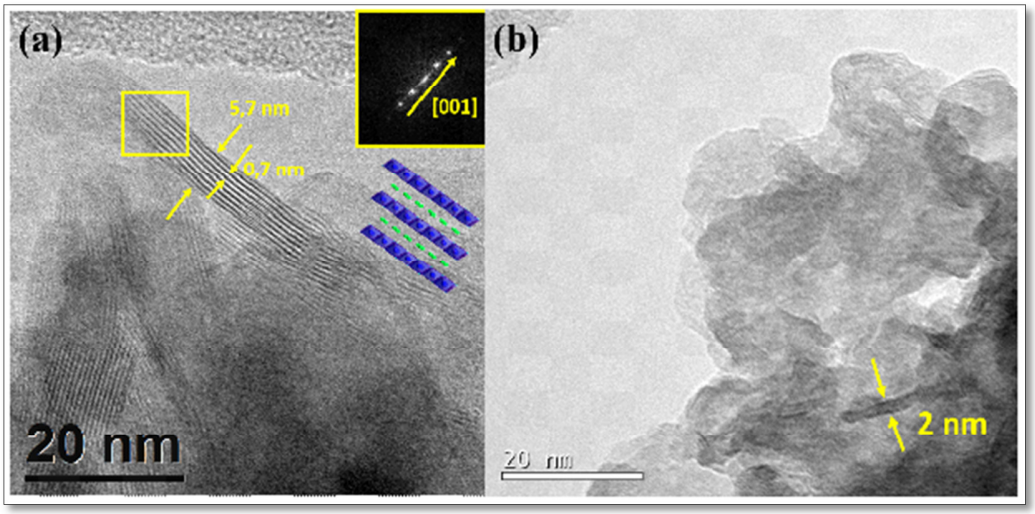

Figure 4. Low magnification images of (a) undoped sample and (b) doped sample with 5% of Fe.

In order to get further structural and compositional information about the cation distribution as well as the transition metal oxidation state, an atomically resolved study was performed in an aberrated corrected Scanning Transmission Electron Microscope (STEM) JEOL JSM-ARM200cF microscope (Cold Emission Gun) combining the HAADF (high annular angle dark field) imaging technique and EELS spectroscopy (Quantum Gif spectrometer). HAADF implies the collection of the electrons scattered at high angles (Solid semi-angles between 68-280 mRad) resulting in incoherent imaging. Under these experimental conditions, the scattered intensity is approximately proportional to Z1.83 (Z=atomic number of the elements in the sample). In this sense, the intensity differences among columns must be related to the different cationic composition, providing images where the column contrast can be qualitatively interpreted as chemical information: the brighter contrast would correspond to heaviest elements while less bright contrast to those elements with lower Z. The incorporation of spherical aberration correctors allows acquiring HAADF images with atomic resolution, making possible to resolve and locate cationic columns with different atomic number, being then an ideal technique for determining the dopant location in original birnessite. Nevertheless, it should be mentioned the high instability of the samples under the focused electron beam, especially in the doped samples, making difficult their characterization. In this scenario, we have explored the use of different acceleration voltages in the range of 200 to 80 kV, being the best results obtained setting the voltage to 80 kV and low electron doses.

A typical HAADF image of an iron doped birnessite **(Figure 5a)** reflects, again, the presence of a very thin matrix oriented along (001) direction and small pieces of layered nanoflakes comprising, in this case, no more than two layers, along the perpendicular direction (schematic structural models have been included). According to the above description of Z contrast imaging, the brightest contrasts must correspond to the heaviest cations, i.e., Mn (Z=25) and/or Fe (Z=26), whereas K (Z=19), in the interlayer space, is not observed due to its low concentration as well as the near presence of Mn/Fe, in the adjacent layers. Nevertheless, it is clear that, in this interlayer position there are not bright contrasts indicating the presence of dopant, i.e., Fe. These experimental observations suggest that Fe should be substituting Mn. The next logical step is trying to elucidate the atomic distribution of the elements simultaneously acquiring the EELS spectra on the area of the layers shown in HAADF. Nevertheless, this is not possible because of the severe damage that this kind of small areas suffers while the beam is scanned during the required time to obtain a good signal-noise ratio spectrum-imaging. Even using short acquisition times (less than 1 min), the scanned area is always destroyed. However, if the EELS spectra are acquired along a line instead of an area, during total exposition times around 30 s, the nanoflakes are not severely damaged. The corresponding EELS sum spectra **(Figures 5b-5d)**, simultaneously acquired along the line marked in the image, evidence the characteristic adsorption edge of the dopant cation, Fe (L3-708 eV), in addition to those of K (L3-296 eV), O (K-510 eV) and Mn (L3-640 eV) of the starting birnessite compound. In addition, the L2,3 Mn fine structure has been analyzed in order to get information of the Mn oxidation state. For that purpose, the position **(Figure 6)** and L2,3 intensity ratio **(Table 1)** of the Mn-L2,3 edge were compared with standards for Mn^{4+} ($Ca_2Mn_3O_8$), Mn^{3+} ($LaMnO_3$) and Mn^{2+} ($CaMnO_2$). Both methods, suggest the coexistence of Mn^{3+} and Mn^{4+}, as can be seen in **Figure 3** and **Table 1**, since the Mn L2,3 edge position and L2,3 intensity ratio of the sample is in between the standards for Mn^{3+} and Mn^{4+}. This result has been obtained either for doped or undoped samples. The oxidation state of Fe cannot be evaluated due to the low signal to noise ratio as consequence of the low Fe concentration.

Table 1. L_3/L_2 intensity ratio.

Sample	**I (L3/L2)**
Birnessite	2.03
$Ca_2Mn_3O_8$ (Mn^{4+})	1.82
$LaMnO_3$ (Mn^{3+})	2.48
$CaMnO_2$ (Mn^{4+})	4.66

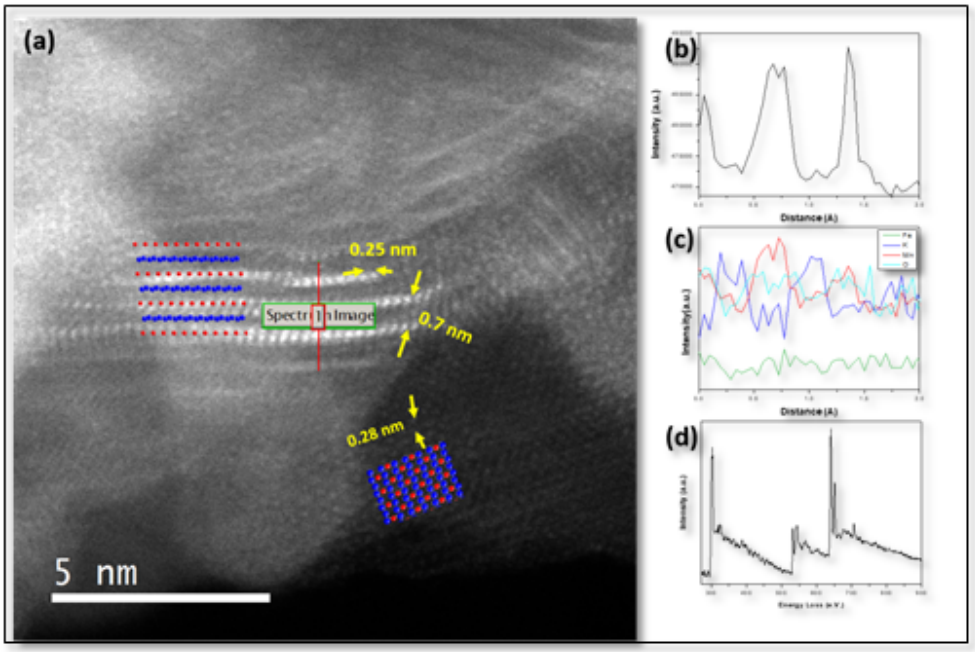

Figure 5. (a) Representative HAADF of a Fe doped birmesite, spectra were acquired along the red line marked in the image. (b) Intensity profile along the line. (c) Intensity profile of the elements. (d) sum spectra; the characteristic lines of the elements are marked.

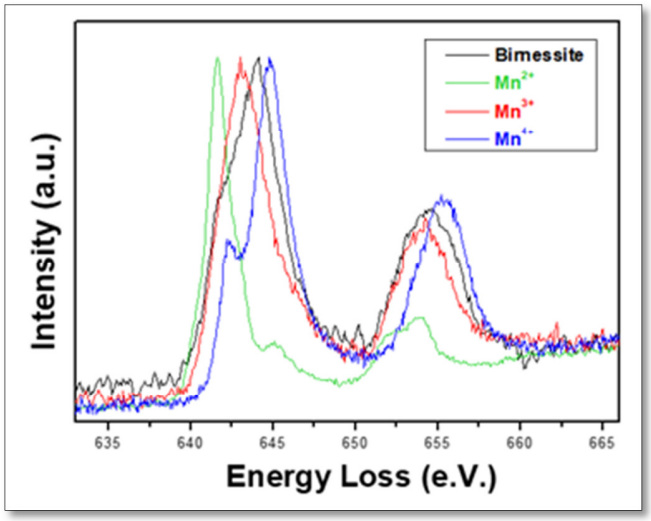

Figure 6. Position of the Mn-$L_{2,3}$ edge compared with standards for Mn^{4+} ($Ca_2Mn_3O_8$), Mn^{3+} ($LaMnO_3$) and Mn^{2+} ($CaMnO_2$).

CONCLUSION

The ensemble of these results shows the optimization of the synthesis and characterization conditions to obtain reproducible nanostructured birnessite doped manganese oxides and to elucidate where these dopants are hosted. Actually, ultrathin (2-4 layers) 5 nm birnessite nanoplatelets, containing Fe, Ti and Ce, can be directly obtained by a room-temperature basic co-precipitation method. The microstructural characterization by means of TEM indicates that the introduction of the dopants previously mentioned leads to the decrease of the particle size of the pure Mn birnessite promoting the orientation of the structure along the c axis. Local EELS compositional analysis confirms the incorporation of dopants in the layered birnessite structure, as well as the coexistence of Mn^{3+} and Mn^{4+} oxidation states. Although it has not been possible to acquire atomically resolved images and EELS chemical maps due to beam damage, the HAADF images of birnessite nanoplatelets oriented along (100) suggest that the interlayer space is free of transition metal atoms. Therefore, the dopants should be located in the manganese positions.

These characterization techniques and synthesis methods can provide an effective tool to design robust functional materials based on birnessite manganese oxide. In the particular case of the electrochemical behavior, the use of these state of art tools could lead to further enhancement of its performance placing these materials as one of the most promising and economic candidates for the next generation of RSOFCs.

ACKNOWLEDGEMENT

This work was supported by the Spanish Ministry of Innovation, Science and Technology and Spanish Ministry of Economy and Competitiveness through Research Projects MAT2014-52405-C02-01 and MAT2017-82252-R.

REFERENCES

1. Royer S, Duprez D, Can F, Courtois X, Batiot-Dupeyrat C, et al. (2014) Perovskites as substitutes of noble metals for heterogeneous catalysis: Dream or reality. Chem Rev 114: 10292-10368.
2. Sengodan S, Choi S, Jun A, Shin TH, Ju YW, et al. (2014) Layered oxygen-deficient double perovskite as an efficient and stable anode for direct hydrocarbon solid oxide fuel cells. Nat Mater 14: 205-209.
3. Cortés-Gil R, Ruiz-González ML, Alonso JM, García-Hernández M, Hernando A, et al. (2011) Magnetoresistance in $La_{0.5}Sr_{0.5}MnO_{2.5}$. Chem Eur J 17: 2709-2715.
4. Yang X, Tang W, Feng Q, Ooi K (2003) Single crystal growth of birnessite- and hollandite-type manganese oxides by a flux method. Cryst Growth Des 3: 409-415.
5. Kingsbury AWG (1956) The rediscovery of Churchite in Cornwall. Mineralogical Magazine 31: 282-282.
6. Post JE, Veblen DR (1990) Crystal structure determinations of synthetic sodium, magnesium and potassium birnessite using TEM and the Rietveld method. Am Mineral 75: 477-489.
7. Post JE (1999) Manganese oxide minerals: Crystal structures and economic and environmental significance. Proc Natl Acad Sci U S A 96: 3447-3454.
8. Thenuwara AC, Cerkez EB, Shumlas SL, Attanayake NH, McKendry IG, et al. (2016) Nickel confined in the interlayer region of birnessite: An active electrocatalyst for water oxidation. Angew Chem Int Ed 55: 10381-10385.
9. Zhu L, Wang J, Rong S, Wang H, Zhang P (2017) Cerium modified birnessite-type MnO_2 for gaseous formaldehyde oxidation at low temperature. Appl Catal B 211: 212-221.
10. Portehault D, Cassaignon S, Baudrin E, Jolivet JP (2008) Design of hierarchical core-corona architectures of layered manganese oxides by aqueous precipitation. Chem Mater 20: 6140-6147.
11. Jenne EA (1968) Trace inorganics in water. USA: American Chemical Society.
12. Prasad VS, Chaudhuri M (1995) Removal of bacteria and turbidity from water by chemically treated manganese and iron ores. Aqua 44: 80-82.
13. Driehaus W, Seith R, Jekel M (1995) Oxidation of arsenate (III) with manganese oxides in water treatment. Water Res 29: 297-305.
14. Prieto O, del Arco M, Rives V (2003) Characterization of K, Na and Li birnessites prepared by oxidation with H_2O_2 in a basic medium. Ion exchange properties and study of the calcined products. J Mater Sci 38: 2815-2824.
15. Bach S, Pereira-Ramos JP, Baffier N (1995) Synthesis and characterization of lamellar MnO_2 obtained from thermal decomposition of NaMnO4 for rechargeable lithium cells. J Solid State Chem 120: 70-73.
16. Zhu K, Guo S, Li Q, Wei Y, Chen G, et al. (2017) Tunable electrochemistry via controlling lattice water in layered oxides of sodium-ion batteries. ACS Appl Mater Interfaces 9: 34909-34914.
17. Yagi H, Ichikawa T, Hirano A, Imanishi N, Ogawa S, et al. (2002) Electrode characteristics of manganese oxides prepared by reduction method. Solid State Ion 154-155: 273-278.
18. Wang H, Li X, Zhou Q, Ming H, Adkins J, et al. (2014) Diversified $Li_{1.2}Ni_{0.2}Mn_{0.6}O_2$ nanoparticles from birnessite towards application specificity and enhancement in lithium-ion batteries. J Alloys Compd 604: 217-225.
19. Conway BE, Pell WG (2003) Double-layer and pseudocapacitance types of electrochemical capacitors and their applications to the development of hybrid devices. J Solid State Electrochem 7: 637-644
20. Wang YG, Wang ZD, Xia YY (2005) An asymmetric supercapacitor using RuO_2/TiO_2 nanotube composite and activated carbon electrodes. Electrochim Acta 50: 5641-5646.
21. Brousse T, Toupin M, Dugas R, Athouël L, Crosnier O, et al. (2006) Crystalline MnO_2 as possible alternative to amorphous compounds in electrochemical supercapacitors. J Electrochem Soc 153: A2171-A2180.
22. Liu L, Min M, Liu F, Yin H, Zhang Y, et al. (2015) Influence of vanadium doping on the supercapacitance performance of hexagonal birnessite. J Power Sources 277: 26-35.

23. Laguna-Bercero MA (2012) Recent advances in high temperature electrolysis using solid oxide fuel cells: A review. J Power Sources 203: 4-16.
24. Thenuwara AC, Shumlas SL, Attanayake NH, Aulin YV, McKendry IG, et al. (2016) Intercalation of cobalt into the interlayer of birnessite improves oxygen evolution catalysis. ACS Catal 6: 7739-7743.
25. Meng Y, Song W, Huang H, Ren Z, Chen SY, et al. (2018) Structure-property relationship of bifunctional MnO_2 nanostructures: Highly efficient, ultra-stable electrochemical water oxidation and oxygen reduction reaction catalysts identified in alkaline media. J Am Chem Soc 136: 11452-11464.
26. McKendry IG, Thenuwara AC, Shumlas SL, Peng H, Aulin YV, et al. (2018) Systematic doping of cobalt into layered manganese oxide sheets substantially enhances water oxidation catalysis. Inorg Chem 57: 557-564.
27. Thenuwara AC, Shumlas SL, Attanayake NH, Cerkez EB, McKendry IG, et al. (2015) Copper-intercalated birnessite as a water oxidation catalyst. Langmuir 31: 12807-12813.
28. Huang H, Meng Y, Labonte A, Dobley A, Suib SL (2013) Large-scale synthesis of silver manganese oxide nanofibers and their oxygen reduction properties. J Phys Chem C 117: 25352-25359.
29. Wang J, Li J, Jiang C, Zhou P, Zhang P, et al. (2017) The effect of manganese vacancy in birnessite-type MnO_2 on room-temperature oxidation of formaldehyde in air. Appl Catal B 204: 147-155.
30. Selvakumar S, Nuns N, Trentesaux M, Batra VS, Giraudon JM, et al. (2018) Reaction of formaldehyde over birnessite catalyst: A combined XPS and ToF-SIMS study. Appl Catal B 223: 192-200.
31. Shen YF, Suib SL, O'Young CL (1996) Cu containing octahedral molecular sieves and octahedral layered materials. J Catal 161: 115-122.
32. Yang X, Tang W, Feng Q, Ooi K (2003) Single crystal growth of birnessite- and hollandite-type manganese oxides by a flux method. Cryst Growth Des 3: 409-413.
33. Feng Q, Yanagisawa K, Yamasaki N (1998) Hydrothermal soft chemical process for synthesis of manganese oxides with tunnel structures. J Porous Mater 5: 153-161.
34. Ching S, Driscoll PF, Kieltyka KS, Marvel MR, Suib SL (2001) Synthesis of a new hollandite-type manganese oxide with framework and interstitial Cr(III) Chem Commun 23: 2486-2487.
35. Zhu S, Li L, Liu J, Wang H, Wang T, et al. (2018) Structural directed growth of ultrathin parallel birnessite on β-MnO_2 for high-performance asymmetric supercapacitors. ACS Nano 12: 1033-1042.
36. Ching S, Petrovay DJ, Jorgensen ML (1997) Sol-gel synthesis of layered birnessite-type manganese oxides. Inorg Chem 36: 883-890.
37. Zhang X, Miao W, Li C, Sun X, Wang K, et al. (2015) Microwave-assisted rapid synthesis of birnessite-type MnO_2 nanoparticles for high performance supercapacitor applications. Mater Res Bull 71: 111-115.
38. Komaba S, Tsuchikawa T, Ogata A, Yabuuchi N, Nakagawa D, et al. (2012) Nano-structured birnessite prepared by electrochemical activation of manganese(III)-based oxides for aqueous supercapacitors. Electrochim Acta 59: 455-463.
39. Liu Z, Ooi K, Kanoh H, Tang W, Tomida T (2000) Swelling and delamination behaviors of birnessite-type manganese oxide by intercalation of tetraalkylammonium ions. Langmuir 16: 4154-4164.
40. Liu Z, Ma R, Ebina Y, Takada K, Sasaki T (2007) Synthesis and delamination of layered manganese oxide nanobelts. Chem Mater 19: 6504-6512.
41. Perreault P, Rifflart S, Nguyen E, Patience GS (2016) Pyrolusite: An alternative oxygen carrier for chemical looping combustión. Fuel 185: 630-638.
42. Pahalagedara L, Kriz DA, Wasalathanthri N, Weerakkody C, Meng Y, et al. (2017) Benchmarking of manganese oxide materials with CO oxidation as catalysts for low temperature selective oxidation. Appl Catal B 204: 411-420.
43. Theofanidis SA, Galvita VV, Konstantopoulos C, Poelman H, Marin GB (2018) Fe-based nano-materials in catalysis. Materials 11: 831.
44. Davis-Gilbert ZW, Tonks IA (2017) Titanium redox catalysis: Insights and applications of an earth-abundant base metal. Dalton Trans 46: 11522-11528.
45. Azor A, Ruiz-Gonzalez ML, Gonell F, Laberty-Robert C, Parras M, et al. (2018) Nickel-doped sodium cobaltite 2D nanomaterials: Synthesis and electrocatalytic properties. Chem Mater 30: 4986-4994.